REPORT

LASER PHYSICS

Widely tunable compact terahertz gas lasers

Paul Chevalier[1], Arman Amirzhan[1], Fan Wang[2], Marco Piccardo[1], Steven G. Johnson[3,4], Federico Capasso[1]*, Henry O. Everitt[5,6]*

The terahertz region of the electromagnetic spectrum has been the least utilized owing to inadequacies of available sources. We introduce a compact, widely frequency-tunable, extremely bright source of terahertz radiation: a gas-phase molecular laser based on rotational population inversions optically pumped by a quantum cascade laser. By identifying the essential parameters that determine the suitability of a molecule for a terahertz laser, almost any rotational transition of almost any molecular gas can be made to lase. Nitrous oxide is used to illustrate the broad tunability over 37 lines spanning 0.251 to 0.955 terahertz, each with kilohertz linewidths. Our analysis shows that laser lines spanning more than 1 terahertz with powers greater than 1 milliwatt are possible from many molecular gases pumped by quantum cascade lasers.

The problem of generating terahertz-frequency radiation (0.3 to 3.0 THz)—in the middle of the electromagnetic spectrum between the microwave region and the infrared (IR) region—has challenged researchers for decades. Not only would wireless communications and radar benefit from operating in the terahertz region, because of appealing characteristics such as high bandwidth, high spatial resolution, compact size, and/or adjustable atmospheric propagation (1), but so would applications requiring stable local oscillators, such as spectroscopy and astronomical observations of the interstellar media. Among the many techniques developed to generate terahertz radiation, the most widely used (2) include harmonic multipliers of tunable microwave sources (3), vacuum electronics (backward-wave oscillators, gyrotrons, and carcinotrons) (4), supercontinua generated by ultrafast lasers and photoconductive switches (5), and difference-frequency mixing of tunable continuous-wave lasers (6–8). Commercial versions of each of these terahertz sources are becoming increasingly available and powerful, but none of them produce much power near 1 THz, and their cost and idiosyncrasies have prevented widespread adoption. Terahertz quantum cascade lasers (9) are compact and can span portions of the region, but they currently have limited fractional tunability (<25%) and operate below room temperature (10, 11).

Often overlooked is one of the earliest sources of terahertz radiation, optically pumped far-infrared (OPFIR) lasers (12). These gas-phase lasers use a discretely line-tunable carbon dioxide (CO_2) laser to excite a specific rotational-vibrational (ro-vibrational) transition in a specific molecular gas to create a rotational population inversion within a tunable cavity. These lasers generate appreciable power (up to 100 mW) and exhibit a narrow linewidth ($\Delta\nu$ < 10 kHz), a combination of features that is not available with most other terahertz sources. However, OPFIR lasers are inefficient, large (~1 m), and require an equally large CO_2 laser and high-voltage power supply. Moreover, they are poorly tunable, requiring the laser gas and CO_2 laser line to be changed each time a different frequency is needed. Consequently, OPFIR lasers fell from widespread use when other sources became available.

Here, we introduce an OPFIR laser concept characterized by frequency tunability over the entire range of rotational transitions from the molecular gas gain medium. Broad terahertz tunability is made possible by using a continuously tunable mid-IR pump source, the quantum cascade laser (QCL) (13). A tunable QCL can optically pump almost any ro-vibrational transition $J_L \rightarrow J_U$ of almost any molecule, thereby promoting population from lower level J_L into a virtually empty excited vibrational level (Fig. 1A). Sufficient pumping of upper level J_U by the QCL inverts the rotational transition $J_U \rightarrow J_U - 1$ and induces this "direct" transition to lase at frequency $\nu \approx 2BJ_U$, where B is the rotational constant of the molecule. The rotational quantum number J_U is selected by the type of ro-vibrational transition excited by the QCL: for P-, Q-, and R-branch transitions, $J_U = J_L -$

1, J_L, and J_L + 1, respectively. With sufficient QCL power, it is also possible to induce the "refilling" transition $J_L + 1 \rightarrow J_L$ to lase, effectively doubling the number of laser lines for a given molecular gas.

The QCL-pumped molecular laser (QPML) is a universal concept: Almost any rotational transition from any molecule with a permanent dipole moment and a vapor pressure can be made to lase if a QCL can be precisely tuned across one of its IR bands. Terahertz lasing was recently reported on several NH_3 transitions near 1.0 THz (14), but we show theoretically and experimentally that the QPML tuning range can be much broader, a 200% fractional tunability covering the entire span of a molecule's rotational spectrum, whose frequencies have been tabulated in several catalogs (15–17). The tuning range for several simple molecules (OCS, N_2O, CH_3F, HCN, and CO) is illustrated in Fig. 1B. Because B is inversely proportional to a principal moment of inertia of the molecule (18, 19), a low moment of inertia molecule like CO has sparser spacing, a broader tuning range, and a peak emission intensity at a high frequency, whereas a higher moment of inertia molecule like OCS has a denser spacing, a narrower tuning range, and a peak at a lower frequency. The number of available transitions increases as the molecular symmetry decreases and molecular mass increases.

Our comprehensive, physics-based multilevel model of the dominant collisional processes shows that OPFIR lasers operate most efficiently in compact cavities, with volumes more than 1000-fold smaller than conventional cavities (20–23). Our compact QPML configuration (Fig. 2A) includes aspects of the cavity design previously reported (20, 22): a 5-mm-diameter, 15-cm-long evacuated copper tube into which is inserted a copper rod rear reflector with a curved face that can be longitudinally scanned until the cavity mode overlaps the gain profile. The output coupler is a 1-mm-diameter pinhole in a flat front plate through which both the QCL and QPML beams propagate. The IR beam from the QCL is focused by a 15-cm-focal-length lens through a Brewster-angled ZnSe window to maximize power into the cavity (typically ~85%), while the terahertz beam diffracts through the pinhole and is refocused into a room-temperature power meter, a Schottky-diode detector, or a receiver operating in the frequency band of interest.

For a given QCL pump power, the terahertz power achievable by this room temperature laser depends on several factors. To ascertain the potential of a given molecular gas as a QPML, consider first the very low-pressure regime in which molecular collisions with the chamber walls occur more frequently than any intermolecular collisions, so a simple three-level model captures the salient behavior. Given that the ~1-MHz QCL linewidth (24) is much less

[1]Harvard John A. Paulson School of Engineering and Applied Sciences, Harvard University, Cambridge, MA 02138, USA. [2]Department of Mechanical Engineering, Massachusetts Institute of Technology, Cambridge, MA 02139, USA. [3]Department of Mathematics, Massachusetts Institute of Technology, Cambridge, MA 02139, USA. [4]Department of Physics, Massachusetts Institute of Technology, Cambridge, MA 02139, USA. [5]U.S. Army Combat Capabilities Development Command Aviation and Missile Center, Redstone Arsenal, AL 35898, USA. [6]Department of Physics, Duke University, Durham, NC 27708, USA.
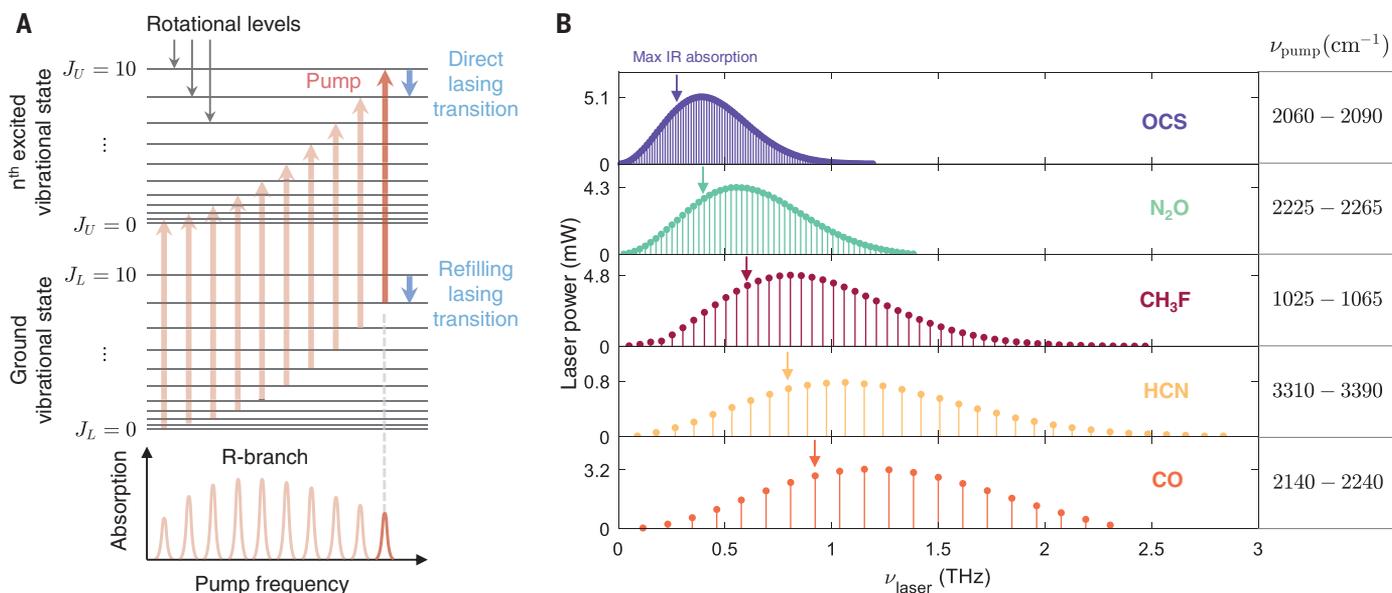*Corresponding author. Email: everitt@phy.duke.edu (H.O.E.); capasso@seas.harvard.edu (F.C.)

Fig. 1. Universality of the quantum cascade laser–pumped molecular laser. (**A**) Diagram showing the rotational levels of a molecule for the ground and excited vibrational states. The red arrows illustrate R-branch transitions $J_L \rightarrow J_U$ responsible for the IR absorption spectrum whose strength depends on the population of each J_L. The blue arrows indicate lasing transitions at frequencies corresponding to an inversion between two rotational states in the excited ("direct") or ground ("refilling") vibrational level. The frequency of the laser emission increases with increasing J_L. (**B**) Plot showing the QCL-pumped molecular laser tuning range and power predicted by the simple model for direct transitions in 20 mTorr of various molecular gases in a compact cylindrical cavity pumped by a 0.25-W QCL: carbonyl sulfide (OCS), nitrous oxide (N_2O), methyl fluoride (CH_3F), hydrogen cyanide (HCN), and carbon monoxide (CO). The arrow indicates the laser transition corresponding to a pump transition from the rotational level with maximum population, illustrating how the Manley-Rowe effect skews the peak power to higher frequency. Also listed is the QCL tuning range required to pump the associated R-branch transitions.

than the ~50- to 150-MHz Doppler width of the IR molecular transition, a simple expression (25) gives the QPML power

$$P_{THz} = \frac{T}{4} \left(\frac{\nu_{THz}}{\nu_{IR}} \right) \left(\frac{\alpha_{IR}}{\alpha_{cell}} \right) [P_{QCL} - P_{th}]$$
$$= \eta [P_{QCL} - P_{th}] \quad (1)$$

and identifies the essential parameters on which it depends at frequency ν_{THz}. Here, α_{IR} is the IR absorption coefficient of the gas molecule at the frequency ν_{IR} to which the QCL is tuned, α_{cell} captures the losses of the cavity, P_{QCL} is the QCL pumping power, and T is the front window transmission coefficient for the terahertz output. For our pinhole coupler with $\nu_{THz} > c/2r_0$, $T \approx (r_0/R_{cell})^2$, where R_{cell} is the cavity radius and r_0 is the radius of the output coupler. Combined, the factors before the square bracket in Eq. 1 constitute the power efficiency η of the QPML. The lasing threshold

$$P_{th} = \frac{h^2}{4\pi} \frac{\nu_{IR}}{\alpha_{IR}} (\alpha_{cell} R_{cell}) \frac{u^2}{|\langle J_U - 1 | \mu | J_U \rangle|^2} \quad (2)$$

depends on many of the same parameters, as well as the average absolute molecular velocity u and the transition dipole matrix element of the rotational transition $\langle J_U - 1 | \mu | J_U \rangle$. As expected, the threshold increases with increasing cavity loss, but the dependence of P_{th} on

cell radius is more subtle because of the strong increase of α_{cell} with decreasing R_{cell} due to ohmic loss (26) experienced by the modes of the hollow metal cavity. The threshold decreases for increasing dipole moment and decreasing ν_{IR}, indicating that terahertz lasing is favored for strongly polar molecules with low frequency vibrational modes.

Equation 1 shows that the maximum power achievable by the QPML, often known as the Manley-Rowe limit (27), is determined by the ratio of the terahertz laser and IR pump frequencies ν_{THz}/ν_{IR}. Any vibrational band may be pumped by the QCL, but this Manley-Rowe limit (27) also recommends low frequency vibrational modes pumped by long-wavelength QCLs. Currently, more powerful QCLs are available at higher frequencies, so the selection of which vibrational mode to excite must be determined by its absorption strength, the Manley-Rowe factor, and the available QCL power.

Moreover, the Manley-Rowe factor indicates that the maximum power of the QPML grows with increasing laser frequency for a given QCL and vibrational band, in great contrast with electronic sources. This Manley-Rowe effect is tempered by the pressure-dependent population n_{J_L}, manifested in the IR absorption term α_{IR}, available for the QCL to excite. One may simply look at the IR spectrum of a molecule to estimate how the power of the corresponding terahertz laser will depend on J_L. However,

the predicted power (Eq. 1) is proportional to the product of α_{IR} and ν_{THz}/ν_{IR}, and Fig. 1B confirms that the peak power occurs when the QCL pumps a transition with higher J_L than the peak of the IR band (where n_{J_L} is maximum) because of this Manley-Rowe effect.

The simple model of Eqs. 1 and 2 captures the molecular and cavity parameters essential for ascertaining how a given molecular gas will perform as a QCL-pumped terahertz laser. Table 1 and Fig. 1B summarize these behaviors for several candidate polar molecules, sorted by threshold pump power. The oblate symmetric top NH_3 has recently been reported as a low threshold QPML near 1 THz (14), and the simple model reveals high power efficiency and large output power from many of these pure inversion transitions (25). However, the other molecules offer much greater tunability, in both range and spacing, and those with large α_{IR} (NH_3, CH_3F, OCS, N_2O, and CO) exhibit many lines with powers above 1 mW.

Because the simple, three-level model in Eqs. 1 and 2 is only valid at very low pressures where there is no collisional quenching of the laser inversion, P_{THz} is predicted to increase linearly with increasing pressure (through α_{IR}). This best-case approximation fails at higher pressures when intermolecular dipole-dipole, rotational-state randomizing, and velocity-randomizing collisions dominate the laser performance and quench the inversion in a manner that depends
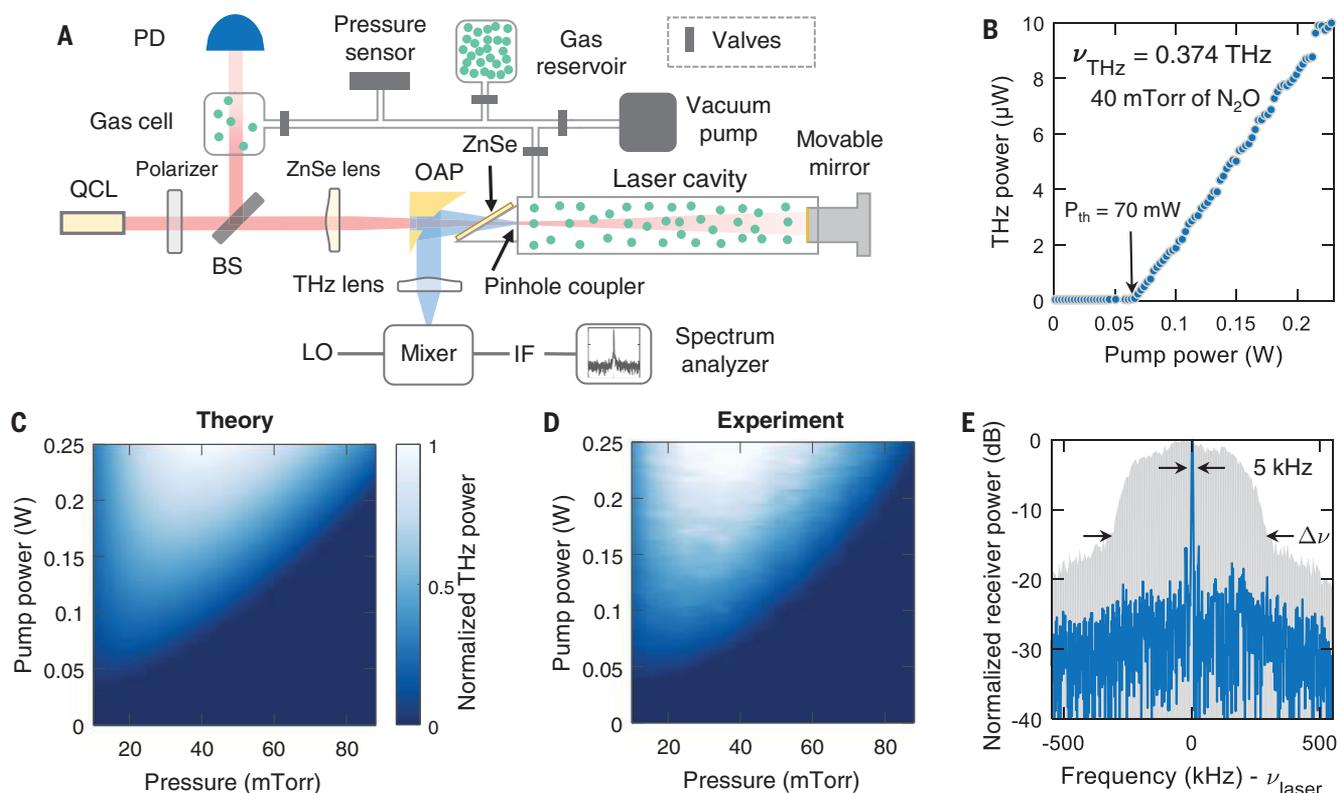
Fig. 2. Experimental setup and results for the N$_2$O molecular laser.
(**A**) Experimental setup: IR light from a widely tunable QCL is tuned to pump a ro-vibrational transition and create a rotational population inversion. Light from the QCL is deflected by a 90%–10% beam splitter (BS) and transmitted through a gas cell so that the QCL may be tuned into coincidence with the vibrational transition by minimizing the transmitted intensity measured using a photodiode (PD). Light is coupled into the laser cavity through a ZnSe window at Brewster's angle and through a pinhole coupler in the cavity. A vacuum pump, pressure sensor, and gas reservoir are used to set the pressure in both the laser cavity and gas cell. The radiation emitted from the pinhole of the QPML is collected with the off-axis parabolic mirror (OAP), focused through a Teflon lens, and measured by a power meter, a detector, or a receiver that uses a frequency-multiplied local oscillator (LO) mixed with the signal to produce the intermediate frequency (IF) measured by a spectrum analyzer. The pump power from the QCL is varied using a wire grid polarizer on a calcium fluoride substrate. The laser cavity is tuned into resonance with the lasing frequency by moving a copper mirror on a translation stage. (**B**) The measured output power of the QPML is plotted as a function of the IR pump power from the QCL. The threshold is P_{th} = 70 mW. After accounting for losses in the collection of the emitted terahertz radiation, the maximum power is ~0.04 mW, and η ≈ 0.2 mW/W at 40 mTorr for the J_U = 15→14 transition at 0.374 THz. Predicted (**C**) and measured (**D**) QPML normalized laser power as a function of gas pressure and QCL pump power for the same direct transition. (**E**) Emission spectrum of the laser (blue line) showing a linewidth of ≤5 kHz at 0.374 THz, corresponding to the J_U = 15→14 transition. The full tuning range of the QPML (broad gray feature) is achieved by varying the cavity length.

on collision cross sections that may not be known. We have previously reported a comprehensive, multilevel model that thoroughly captures these behaviors, finding that the IR-to-terahertz photon conversion efficiency of an optimized CH$_3$F OPFIR laser may exceed 30% (23). This model has been adapted to predict the performance of QPMLs as a function of P_{QCL} and pressure (25).

To illustrate the performance and tunability of a compact QPML, we chose nitrous oxide (N$_2$O), whose v_3 vibrational mode falls within the 2119 to 2342 cm^{-1} tuning range of our 320-mW QCL. The spacings of the N$_2$O lasing transitions are ~$2B_{N_2O}$ = 25.1 GHz, and the frequency span over which this QPML may be tuned is ~1.5 THz. QCL frequency tuning was accomplished by monitoring the IR signal transmitted through a separate 15-cm gas cell

containing 50 mTorr of N$_2$O using a HgCdTe detector. The QCL frequency was tuned by precise temperature control until molecular absorption minimized the transmitted IR power (Fig. 2A). Here, we will refer to lasing transitions (both direct and refilling) by the quantum number J_L of the lower level drained by the IR pump.

We observed lasing for all 29 direct lasing transitions (Fig. 3A), as well as eight refilling transitions (Fig. 3B), between 0.251 and 0.955 THz (corresponding to 9 ≤ J_L ≤ 37) by exciting each R-branch v_3 ro-vibrational transition over a QCL tuning range of 2231 to 2250 cm^{-1}. Refilling transitions and direct transitions corresponding to the same J_L exhibit slightly different frequencies owing to different B rotational constants for the ground and excited vibrational states. Lasing below 0.251 THz could

not be observed because it occurred below the radiation-suppressing cutoff frequency of the pinhole output coupler. For most transitions, we measured the strength of the laser emission as a function of pressure for maximum QCL pumping power, and in some cases we also measured the laser emission as a function of QCL pumping power (see Fig. 2B for J_L = 14). From these measurements, we were able to obtain the threshold power P_{th} and power efficiency η of many laser lines (25), providing critical information for ascertaining the molecular dipole-dipole and thermalizing gas kinetic collisional cross sections needed in the comprehensive model (22, 23, 28).

We also used heterodyne receivers operating between 0.300 and 0.775 THz to measure the spectrum of these laser transitions (see Fig. 2E for the recovered line at v_{THz} = 0.374 THz).

Table 1. Predicted QPML power (Eq. 1) and QCL threshold pump power (Eq. 2) for the highest power lasing transition of nine candidate laser molecules at 20 mTorr. Assumes a 0.25-W QCL pumping through a 1-mm-diameter pinhole output coupler into a 5-mm-diameter cylindrical laser cavity (loss = 0.06 m^{-1}) containing the molecular gas with dipole moment μ. With optimized pressure, even higher power is achievable (*23*).

Molecule	J_L (peak)	ν_{THz} (THz)	P_{THz} (mW)	P_{th} (mW)	η (mW/W)	μ (D)	ν_{IR} (cm^{-1})	α_{IR} (m^{-1})
CH$_3$F	15	0.806	4.8	0.041	19.2	1.85	1072.774	4.59
NH$_3$	3	1.073	16.7	0.056	66.6	1.46	967.346	10.8
OCS	31	0.389	5.2	0.069	20.5	0.72	2073.894	19.6
HCN	11	1.063	0.8	0.164	3.11	2.98	1447.962	0.76
H$_2$CO	13	1.087	0.8	0.218	3.28	2.33	1776.861	0.96
CH$_3$^{35}Cl	20	0.558	0.04	2.42	0.14	1.90	1459.582	0.07
N$_2$O	21	0.553	4.3	3.14	17.4	0.17	2240.439	12.7
CH$_3$OH	15	2.523	0.2	4.88	0.92	1.41	1031.477	0.07
CO	9	1.153	3.2	27.2	14.5	0.12	2179.772	4.93
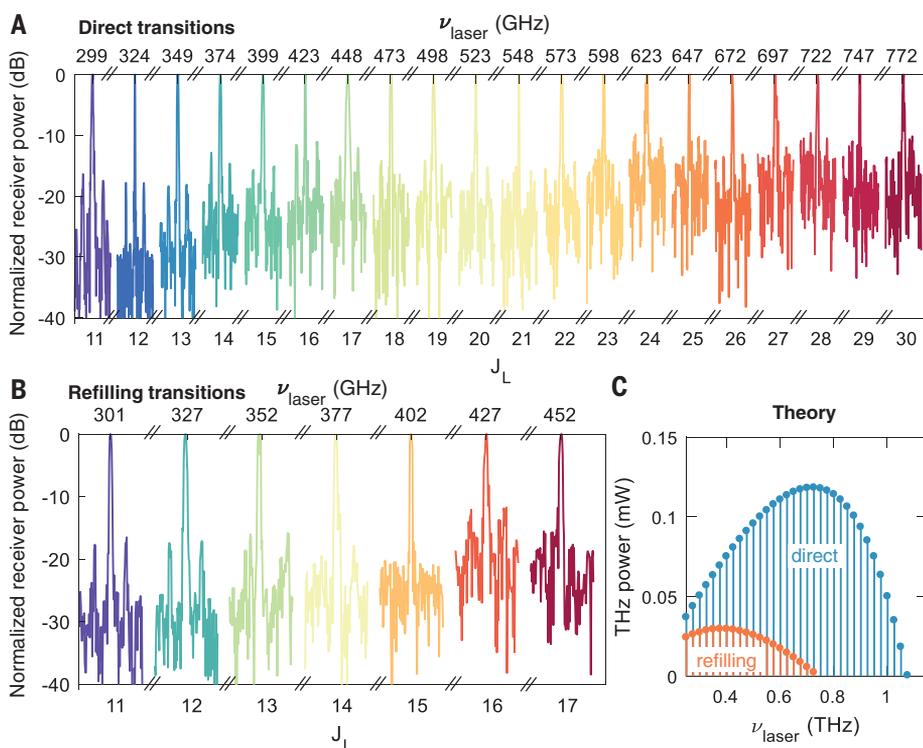
Fig. 3. Tunability of the optically pumped N$_2$O laser. Emission spectra of the laser were measured as the QCL pump laser was tuned to different IR transitions of N$_2$O. The x axes show the measured emission frequency and the associated quantum number J_L of the lower level of the pumped R-branch transition. The QCL power was maximal (up to 0.25 W coupled in the cavity), and the pressure was 40 mTorr for direct transitions and 20 mTorr for refilling transitions. (**A**) Measured spectra of direct transitions with J_L from 11 to 30. (**B**) Measured spectra of refilling transitions with J_L from 11 to 17. (**C**) The output power of the laser predicted by the comprehensive model (*23*) using the deduced collisional parameters of N$_2$O and the estimated cavity losses, plotted as a function of frequency for the optimal pressure.

The instantaneous linewidths were <1 kHz, but because of frequency jitter the effective linewidths were typically 3 to 6 kHz. Other measured lines are shown in Fig. 3, A and B, over a 200-kHz span. We were able to demonstrate frequency tuning of the laser across its full Doppler-broadened gain bandwidth by precisely adjusting the cavity length with a motorized micrometer. The broad feature (gray curve) in Fig. 2E envelopes the range of individual frequencies over which the laser was tuned while keeping the pump laser at a constant power and frequency. Importantly, the QPML frequency was quite stable (routinely <10 kHz) while freely running and could be made even more stable through active frequency stabilization of the QCL (*29*) and the laser cavity (*30*).

Constrained by these experimental measurements of terahertz power as a function of pressure and pump power, our comprehensive theoretical model (*23*) was able to estimate the collisional cross sections and predict the optimal performance of the laser. The dipole-dipole collisional cross section was estimated to be 35 Å^2, well within the expected range (*25*), while the cavity loss (α = 0.3 m^{-1} at 374 GHz) was estimated to be five times higher than the theoretical minimum (*25*). Figure 2, C and D, respectively, reveal the excellent agreement between the predicted and measured output terahertz power for J_L = 14 as a function of N$_2$O pressure and QCL pump power. The model predicts, and measurements confirm, that the optimal and maximum pressure for laser operation increases with increasing J_L (*25*), a consequence of the increasing Doppler width of the gain profile with increasing laser frequency.

The comprehensive model was used to predict the expected laser power for each transition at its optimal gas pressure, and Fig. 3C shows that the direct lasing transition with maximum power occurs not for J_L = 15, where n_{J_L} is largest, but for J_L = 28 because of the Manley-Rowe effect. While the output power increased as a function of the frequency, the signal-to-noise ratio in the heterodyne measurement (Fig. 3, A and B) was limited by the decreasing efficiency of the electronic subterahertz source. An emitted power of 69 μW was predicted for the J_L = 14, ν_{THz} = 0.374 THz direct transition. Although we measured only 10 μW (Fig. 2B), our power measurements underestimate the emitted power by at least a factor of four, for reasons including significant diffraction of the emitted terahertz beam beyond the collection optics, absorption and reflection by the ZnSe Brewster window and Teflon lens, and use of the power meter at the edge of its calibrated range.

Like traditional OPFIR lasers, QPMLs exhibit high brightness temperatures $T_b = Ic^2/(2k\nu_{THz}^2\Delta\nu) > 10^{14}$ K for laser radiance I = 1 mW·cm^{-2}·sr^{-1} (where k is the Boltzmann constant, c is the speed of light, and $\Delta\nu$ = 1 kHz the linewidth). Because our theoretical models and experimental demonstrations with N$_2$O confirm the universal concept of a terahertz molecular laser source broadly tunable across its entire rotational manifold when pumped by a continuously tunable QCL, the outlook for QPMLs is indeed very bright.

REFERENCES AND NOTES

1. T. Nagatsuma, G. Ducournau, C. C. Renaud, *Nat. Photonics* **10**, 371–379 (2016).
2. R. A. Lewis, *J. Phys. D Appl. Phys.* **47**, 374001 (2014).
3. A. Maestrini *et al.*, *IEEE Trans. Microw. Theory Tech.* **58**, 1925–1932 (2010).
4. J. H. Booske *et al.*, *IEEE Trans. Terahertz Sci. Technol.* **1**, 54–75 (2011).
5. Y. Shen, P. Upadhya, E. Linfield, H. Beere, A. Davies, *Appl. Phys. Lett.* **83**, 3117–3119 (2003).
6. K. McIntosh *et al.*, *Appl. Phys. Lett.* **67**, 3844–3846 (1995).
7. K. Evenson, D. Jennings, F. Petersen, *Appl. Phys. Lett.* **44**, 576–578 (1984).
8. M. Inguscio, P. D. Natale, L. Veseth, *Comments At. Mol. Phys.* **30**, 3 (1994).
9. R. Köhler *et al.*, *Nature* **417**, 156–159 (2002).
10. L. Bosco *et al.*, *Appl. Phys. Lett.* **115**, 010601 (2019).
11. C. A. Curwen, J. L. Reno, B. S. Williams, *Nat. Photonics* 10.1038/s41566-019-0518-z (2019).
12. T. Chang, T. Bridges, E. Burkhardt, *Appl. Phys. Lett.* **17**, 249–251 (1970).
13. J. Faist *et al.*, *Science* **264**, 553–556 (1994).
14. A. Pagies, G. Ducournau, J.-F. Lampin, *APL Photonics* **1**, 031302 (2016).
15. I. Gordon *et al.*, *J. Quant. Spectrosc. Radiat. Transf.* **203**, 3–69 (2017).
16. JPL Molecular Spectroscopy Database (2017); https://spec.jpl.nasa.gov/.
17. Splatalogue Database for Astronomical Spectroscopy (2007); www.cv.nrao.edu/php/splat/.
18. C. Townes, A. L. Schawlow, *Microwave Spectroscopy* (Dover Publications, 1995).
19. W. Gordy, R. L. Cook, *Microwave Molecular Spectroscopy* (Wiley-Interscience, 1984).
20. H. O. Everitt, D. D. Skatrud, F. C. DeLucia, *Appl. Phys. Lett.* **49**, 995–997 (1986).
21. R. McCormick, H. Everitt, F. DeLucia, D. Skatrud, *IEEE J. Quantum Electron.* **23**, 2069–2077 (1987).
22. S.-L. Chua *et al.*, *Opt. Express* **19**, 7513–7529 (2011).
23. F. Wang *et al.*, *Proc. Natl. Acad. Sci. U.S.A.* **115**, 6614–6619 (2018).
24. K. Knabe *et al.*, *Opt. Express* **20**, 12432–12442 (2012).
25. See supplementary materials.
26. R. Bansal, *Fundamentals of Engineering Electromagnetics* (CRC Press, 2006).
27. J. Manley, H. Rowe, *Proceedings of the IRE* **44**, 904–913 (1956).
28. H. O. Everitt, F. C. De Lucia, *Adv. At. Mol. Opt. Phys.* **35**, 331–400 (1995).
29. R. M. Williams *et al.*, *Opt. Lett.* **24**, 1844–1846 (1999).
30. R. L. Crownover, H. O. Everitt, F. C. De Lucia, D. D. Skatrud, *Appl. Phys. Lett.* **57**, 2882–2884 (1990).

Science

Widely tunable compact terahertz gas lasers

Paul Chevalier, Arman Amirzhan, Fan Wang, Marco Piccardo, Steven G. Johnson, Federico Capasso and Henry O. Everitt

Filling the terahertz gap
Compared with other wavelengths, coherent sources of electromagnetic radiation in the terahertz regime are relatively scarce. Despite a number of applications in security imaging, spectroscopy, and chemical analysis, it has been experimentally challenging to produce such light. Chevalier *et al.* demonstrate an approach involving the excitation of a molecular gas with a quantum cascade laser. They show that they can tune into a broad range of desired wavelengths by carefully selecting the required molecular transition. A compact platform—the size of a shoe box—and widely tunable source of coherent terahertz radiation should find immediate application across a number of fields.
Science, this issue p. 856

ARTICLE TOOLS	http://science.sciencemag.org/content/366/6467/856
SUPPLEMENTARY MATERIALS	http://science.sciencemag.org/content/suppl/2019/11/13/366.6467.856.DC1
REFERENCES	This article cites 30 articles, 2 of which you can access for free http://science.sciencemag.org/content/366/6467/856#BIBL
PERMISSIONS	http://www.sciencemag.org/help/reprints-and-permissions

Use of this article is subject to the Terms of Service